Scenarios for the onset of convection close to the critical point

Laurence El Khouri and Pierre Carlès
Laboratoire de Modélisation en Mécanique, Université Pierre et Marie Curie, Case 162, 4 place Jussieu, 75252 Paris Cedex 05, France

(Received 2 January 2002; published 30 December 2002)

We perform a theoretical analysis of the onset of convection in a layer of near-critical ^{3}He submitted to an unsteady bottom heating. A theoretical model previously presented [P. Carlès, Physica D **147**, 36 (2000)] is adapted to the corresponding physical conditions, and a method is proposed to solve the associated equations. We predict, for different intensities of heating and different initial temperatures, when convection will start and what will be the shape of the dominant growing perturbations. A systematic parametric analysis shows that the onset of convection in a supercritical fluid can take place following four distinct scenarios, depending on the initial temperature and the intensity of the heating. Two of these scenarios are entirely specific to near-critical fluids, being impossible to observe in classical Boussinesq fluids.

DOI: 10.1103/PhysRevE.66.066309 PACS number(s): 44.25.+f, 47.20.Bp, 47.27.Te, 47.40.−x

Fluids near the liquid-vapor critical point are at the same time dense and highly compressible. The onset of convection in such systems is a very active subject of research, mainly for two reasons. First, the hydrodynamics of these fluids is an interesting problem in itself, owing to their numerous industrial applications as well as their importance in terms of fundamental physics. But also, several authors have shown in recent years that supercritical fluids, under certain conditions, could be used as scaled-down laboratory models for large geophysical flows [1–4]. This last consideration has been a strong incentive for the study of gravity-linked phenomena in supercritical fluids such as internal gravity waves and the Rayleigh-Bénard convection. The results presented in this paper aim at shedding some light on the sequence of events which drive a bottom-heated supercritical fluid layer into the convective regime.

It has been shown in recent years that fluids near their critical point are subjected to a specific temperature relaxation mechanism called the piston effect (PE), which becomes increasingly efficient as the critical point is approached [5–8]. This mechanism can be described as follows: when a sample of near-critical fluid confined in a fixed-volume container is locally heated, a thermal boundary layer forms close to the heated zone; due to the large compressibility of the fluid, this boundary layer expands and acts as a piston, driving an isentropic compression of the rest of the fluid; as a consequence, the temperature in the whole sample rises in a rapid and homogeneous way. In the presence of gravity, the hot fluid in the boundary layer has a tendency to rise as a result of buoyancy forces, so that a subtle interplay takes place between PE and buoyancy-driven convection. This interplay is the source of a great variety of behaviors as regards the Rayleigh-Bénard stability of a fluid close to the critical point, the problem under study here.

Rayleigh-Bénard stability of near-critical fluids was first studied in the pioneering works of Giterman and Steinberg [9]. Recently, a renewed interest for near-critical hydrodynamics drove experimenters, numericists, and theorists into revisiting this problem. Several experimental studies showed the relevance of Giterman and Steinberg's first results [10,2,11], while a more concise theoretical approach of the stability problem was proposed by Carlès and Ugurtas [12]. Through all these works, it has been demonstrated that the criteria for the onset of convection in a supercritical fluid subjected to an adverse temperature gradient is

$$\mathrm{Ra}^{Corr} > \mathrm{Ra}_c , \tag{1}$$

where Ra^{Corr} is defined as the classical Rayleigh number, in which the temperature gradient dT/dz is replaced by $dT/dz+\mathcal{G}$. $\mathcal{G}$ is the adiabatic temperature gradient, defined as $\mathcal{G}=\rho g(\partial T/\partial P)_s$. Ra_c is a critical Rayleigh number depending on the boundary conditions and having the same values as in the Boussinesq case [12,13]. The theoretical criterion in Eq. (1) is based, however, on somewhat unphysical initial conditions: the fluid is supposed to be in a state of stationary conduction, and the convective stability of this initial state is explored. In real experiments however, the fluid is generally at a constant initial temperature and is gradually heated from the bottom, until eventually a steady regime of conduction is reached. The transients observed during this heating process (governed by PE close to the critical point) may themselves be subjected to convective instabilities. Consequently, the final regime of conduction is practically observed only in the stable case: in the unstable case, convection ensues before this steady regime is reached. The theoretical models mentioned above [9,12], based on stationary initial conditions, are thus unable to describe the influence of PE on the onset of convection.

In order to go beyond these limitations, a stability analysis based on the more physical case of an unsteady bottom heating was proposed by Carlès [14], in which the competition between PE and natural convection was studied in a quantitative way. In the present work, we adapt this unsteady model to the case of a bottom-heated layer of near-critical ^{3}He. We check the Rayleigh-Bénard stability of the fluid layer for different values of the initial temperature and for different intensities of heating. Analyzing the morphology of the fluid flow generated by the growing perturbations in the unstable cases, we identify four distinct scenarios which describe how convection sets in in a bottom-heated near-critical fluid.

Let us first examine the model and its adaptation to the case of the ^{3}He layer. The specific parameters and boundary conditions used here are chosen so as to match the characteristics of the experiment of Kogan and co-workers [11,3], a choice which should make future experimental comparisons easier. We thus consider a supercritical layer of ^{3}He confined between two infinite horizontal plates separated by a gap of length $L=1.06$ mm. The fluid is initialy at critical density ($\rho_c=41.45\ \mathrm{kg\,m^{-3}}$) and at a temperature T_i slightly above the critical temperature ($T_c=3.316$ K). The reduced temperature is defined in the usual way as $\varepsilon=(T_i-T_c)/T_c$. The temperature of the top plate is regulated at T_i, and at a given time a constant heat flux q is applied at the bottom plate. This bottom-heating drives a PE flow in the fluid layer, and the stability of this flow versus natural convection is analyzed for different values of ε and q as time elapses.

The problem is first rewritten in nondimensional form using the following variables and unknowns [with the space variables (x,y,z), time t, and (u,v,w) the components of velocity]:

$$T^*=T/T_c,\quad P^*=P/P_c,\quad \rho^*=\rho/\rho_c,$$
$$(u^*,v^*,w^*)=(u,v,w)/V_{ref},\qquad (2)$$
$$(x^*,y^*,z^*)=(x,y,z)/L\quad t^*=tV_{ref}/L,$$

with $V_{ref}=\eta/(\rho_c L)$ the speed of viscous diffusion (with eta the shear viscosity). The reason of this unusual reference choice is explained in Ref. [12]. The PE flow (which is the base flow of the present stability analysis) is found analytically like in Ref. [14] for the particular set of boundary conditions considered here: a prescribed heat flux at the bottom and a regulated temperature at the top. The associated base temperature profile is denoted by $T_B^*(z^*,t^*)$. Small three-dimensional perturbations are added to this base flow, and the nondimensional equations describing their evolution are shown to be [14] (subscripts indicate partial derivatives and stars have been omitted)

$$\Delta w_t=\beta_P\Delta_h\tau+\Delta^2 w, \qquad (3)$$

$$\tau_t=-\frac{1}{\mathrm{Fr}^2}(T_{Bz}+g)w+\frac{1}{\mathrm{Pr}}\Delta\tau, \qquad (4)$$

with w the perturbation of vertical velocity and τ the temperature perturbation. $\beta_P=-(T_c/\rho_c)(\partial\rho/\partial T)_P$ (nondimensional isobaric expansion coefficient), $\mathrm{Fr}=V_{ref}/\sqrt{gL}$ (Froude number), $\mathrm{Pr}=\eta C_P/\lambda$ (Prandtl number), and $g=\mathcal{G}(L/T_c)$ (nondimensional adiabatic temperature gradient). Δ_h is the Laplacian operator taken in the horizontal plane (x, y) only. With Eqs. (3) and (4) are associated boundary conditions on w and τ which describe the nature of the boundaries (solid plates) and their thermal behavior (isothermal at the top, with imposed heat flux at the bottom) (see Chandrasekhar [13] for more details). As can be seen in Eqs. (3) and (4), the stability of the fluid layer is governed by the specific temperature profile created by the piston effect. An example of such a profile is given in Fig. 1(c). A typical two-boundary layers pattern is observed: a thermal boundary layer appears at the bottom, where the fluid is heated by the lower plate; this heating drives a PE which increases the bulk temperature beyond that of the upper plate, and a second boundary layer appears on top of the cell where the fluid is cooled by the upper plate. The thermal configuration is thus potentially unstable in both of these layers [14].

In order to solve Eqs. (3) and (4) for the associated boundary conditions, solutions are first decomposed in the horizontal plane as periodic Fourier components of wave numbers k_x in the x direction and k_y in the y direction. The time dependence of these Fourier modes is then assumed to be exponential, an assumption equivalent to applying the classical hypothesis of *frozen base flow* to the PE base flow: T_B is assumed to be a function of a ''slow'' time parameter t_0 (the time at which the base flow is observed), and the perturbations to be functions of a ''fast'' time variable t, independent of t_0. The application of this hypothesis in the present context raises several complex issues which are discussed in Ref. [14]. w and τ are thus defined as

$$w(x,y,z,t)=\tilde{w}(z)\ e^{\sigma(t-t_0)}e^{i(k_x x+k_y y)}, \qquad (5)$$

$$\tau(x,y,z,t)=\tilde{\tau}(z)e^{\sigma(t-t_0)}e^{i(k_x x+k_y y)}, \qquad (6)$$

and their governing equations become

$$\sigma(\tilde{w}_{zz}-k^2\tilde{w})=\beta_P k^2\tilde{\tau}+(\tilde{w}_{zzzz}-2k^2\tilde{w}_{zz}+k^4\tilde{w}), \qquad (7)$$

$$\sigma\tilde{\tau}=-\frac{1}{\mathrm{Fr}^2}\left[T_{Bz}(z,t_0+\mathcal{G}]\tilde{w}+\frac{1}{\mathrm{Pr}}(\tilde{\tau}_{zz}-k^2\tilde{\tau}).\right. \qquad (8)$$

$k=\sqrt{k_x^2+k_y^2}$ is the wave number of the perturbation, σ its growth rate. Equations (7) and (8) and the associated boundary conditions define an eigenvalue problem linking σ and k for a given t_0. In order to solve this problem, the following numerical procedure is applied. The fluid cell is first discretized with N mesh points, and a $2N$ vector V is defined as $V=(\tilde{w}(1/N),\ldots,\tilde{w}(1),\tilde{\tau}(1/N),\ldots,\tilde{\tau}(N))$. Equations (3) and (4) and the associated boundary conditions are then discretized using finite differences for derivation operators, which finally yields the following relationship:

$$\sigma A_k V=B_k V, \qquad (9)$$

where A_k and B_k are two $(2N,2N)$ matrices, functions of k and t_0 (and of the nondimensional numbers characterizing the physical problem). Equation (9) defines a generalized eigenvalue linear problem, where the σ's are the generalized eigenvalues (corresponding to the rates of growth of perturbations of wave vector k) associated with generalized eigenvectors V_σ (corresponding to the shape of the associated velocity and temperature perturbations). Thus, at any given time t_0 during the heating, it is possible to check the stability of perturbations of any wave number k and predict the shape of the most unstable ones by looking at the corresponding eigenvector V_σ. The time of onset of convection t_{ons} can be found as the first value of t_0 for which there exists at least one value of k leading to a growth rate σ with a positive real

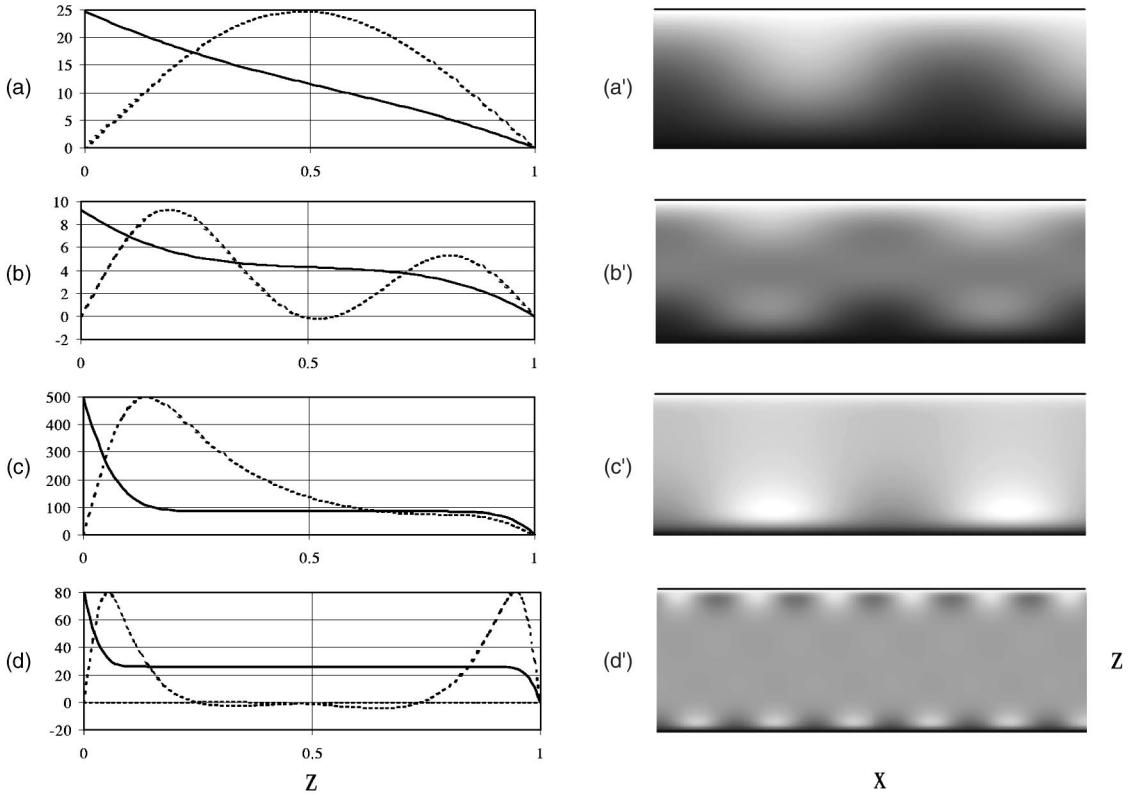

FIG. 1. Base temperature profiles (solid lines) and temperature perturbations (dotted lines) at the time of convection onset for each scenario (a)–(d); (temperature profiles are plotted in microkelvins while the amplitude of the perturbation is arbitrary); associated temperature fields shortly after the onset (a′)–(d′); (black is hot, white is cold, and only a $4L$-wide portion of the infinite fluid layer is represented); the associated experimental conditions are detailed in the core of the text.

part. The type of growing perturbations observed in the fluid layer at this moment can also be predicted: it is described by the associated eigenvector V_σ, whose first N components represent the shape of the most unstable velocity perturbation w and last N components represent the shape of the associated temperature perturbation τ. The accuracy of this procedure was checked on the basis of the classical Rayleigh-Bénard problem in Boussinesq fluids. The first few eigenmodes of the discrete system converged to the first few eigenmodes of the continuous system (as found in Ref. [13]) when N was increased. The accuracy was found satisfactory even for small values of N (a few tens).

Using the procedure just described, we performed a systematic analysis of the stability of the ^{3}He layer for a wide range of heat fluxes q and reduced temperatures ε. For each pair of parameters, we calculated the time of onset t_{ons} and the shape of the most unstable perturbation (obtained from the corresponding eigenvector V_σ). The different types of growing perturbations could be sorted into only four distinct classes, each class describing a possible scenario for the transition from PE to convection.

Let us first define the critical heat flux q_c as the flux which drives the fluid layer exactly on the convective threshold when it reaches its final regime of steady conduction.

Scenario (a): *q close to q_c any value of ε*. The first scenario is observed when the heat flux is such that convection ensues at a time when the upper and lower boundary layers have already reached each other in their process of diffusion. At this time, an almost constant temperature gradient is established in the cell. The stability problem is then very similar to that studied in Refs. [9,12]: the most unstable wave number k is of order 3 and the associated perturbation occupies the whole fluid layer. An example of the corresponding base temperature profile $T_B(z)$ and of the most unstable temperature perturbation is plotted in Fig. 1(a) for $\varepsilon=0.1$ and $q=6.22\times10^{-4}$ Wm^{-2} (which leads to $t_{ons}=12$ s for $k=3$). In Fig. 1(a′) a temperature field has been drawn based on the superposition of $T_B(z)$ and of the most unstable temperature perturbation [as defined in Eq. (6), with a small amplitude arbitrarily chosen]. This figure gives a visual idea of the type of temperature field which should be observed in the fluid layer shortly after the onset. It would be interesting to compare such plots with the temperature fields predicted by the numerical simulations of Chiwata and Onuki [15] or Amiroudine and co-workers [16].

Scenario (b): *q close to q_c [higher than in scenario (a)], any value of ε*. When the heat flux is a little higher than in scenario (a), convection sets in a short time before the two boundary layers meet. In this situation, both boundary layers destabilize at the same time in a coupled manner: the most unstable perturbation corresponds to a coupled pair of perturbations located in each boundary layer. The most unstable wave number is typically between 4 and 6. Examples of the base temperature profile and of the temperature perturbation

for such a scenario are plotted in Fig. 1(b) for $\varepsilon=0.02$, $q=5.1\ 10^{-4}\ \mathrm{W\,m^{-2}}$ (which leads to $t_{ons}=14$ s for $k=4$). The temperature field shortly after the onset is drawn in Fig. 1(b′): the coupled deformation of the two boundary layers can be clearly observed.

Scenarios (a) and (b) are observed when q is close to q_c. If $q \gg q_c$, then convection starts when the boundary layers still occupy only a fraction of the whole fluid cell. Both boundary layers are potentially unstable, the bottom one being always more unstable than the top one. Two cases are observed depending on the initial temperature, leading to scenarios (c) and (d).

Scenario (c): $q \gg q_c$, $\varepsilon \gg 0.01$. Far from the critical point, the bottom boundary layer is unstable at the time of onset while the top one remains stable. Convection starts at the bottom and develops before the top boundary layer becomes unstable. The most unstable wave number is then of the order of $3L/\delta$, where Δ is the boundary layer thickness at t_{ons}. Such a situation is represented in Figs. 1(c) and (c′) for $\varepsilon=0.2$ and $q=0.1\ \mathrm{W\,m^{-2}}$ (which leads to $t_{ons}=0.2$ s for $k=3.8$).

Scenario (d): $q \gg q_c$, $\varepsilon \lesssim 0.01$. Close to the critical point, the top and bottom boundary layers are symmetrical and both unstable at the time of onset: convection starts from the top and the bottom of the layer in a simultaneous way. The most unstable wave number is, again, of the order of $3L/\delta$, but this time two unstable symmetric perturbations appear at almost the same time, one located in the bottom boundary layer and the other in the top one. These two modes of perturbations however are not coupled, unlike what happens in scenario (b): each boundary layer behaves independently, as if the other layer did not exist. This situation is represented in Fig. 1(d) and (d′) for $\varepsilon=0.01$ and $q=3.3\times10^{-2}\ \mathrm{W\,m^{-2}}$ (which leads to $t_{ons}=0.62$ s for $k=11.5$). Such a scenario has recently been observed in numerical simulations of van der Waals fluids by Amiroudine *et al.* [16].

Note that among the four possible scenarios, only scenarios (a) and (c) can be observed in fluids far from the critical point for the same heating conditions. In scenarios (b) and (d) indeed, growing perturbations appear at the same time at the bottom and at the top of the fluid layer, although only the bottom is heated. Such a situation is possible only thanks to PE: it can be observed only in the vicinity of the critical point.

In conclusion, we have developed a theoretical model for analyzing the unsteady Rayleigh-Bénard stability of near-critical fluids layers and applied it to a set of parameters matching recent experiments on ^{3}He [11,3]. The model enables the prediction of the time of onset of convection and of the morphology of the fluid flow which follows. Four distinct scenarios have been identified, describing how convection sets in a bottom-heated supercritical fluid. Given an experimental setup, our model is able to predict if convection will start during the bottom heating, when it will start, and which scenario will be observed at the onset. Experimental comparisons with the results of Kogan and Meyer are presently under way, and the transition between the scenarios in a (q,ε) diagram is being investigated.

We would like to acknowledge Dr. Ivan Delbende from LIMSI (Orsay, France) for his fruitful advice on the resolution of dispersion equations. We feel extremely indebted to Professor Horst Meyer and Dr. Andrei Kogan for regular discussions about their experimental results and for communicating data on ^{3}He.

[1] R.F. Berg, M.J. Lyell, G.B. McFadden, and R.G. Rehm, Phys. Fluids **8**, 1464 (1996).
[2] X. Chavannes, Ph.D. dissertation, Université Joseph Fourier, Grenoble, France, 1997 (unpublished).
[3] A.B. Kogan and H. Meyer, Phys. Rev. E **63**, 056310 (2001).
[4] P. Carlès and L. El Khouri, Phys. Fluids **13**, 3775 (2001).
[5] A. Onuki (private communication).
[6] A. Onuki, H. Hao, and R.A. Ferrell, Phys. Rev. A **41**, 2256 (1990).
[7] H. Boukari, J.N. Shaumeyer, M.E. Briggs, and R.W. Gammon, Phys. Rev. A **41**, 2260 (1990).
[8] B. Zappoli, D. Bailly, Y. Garrabos, B. Le Neindre, P. Guenoun, and D. Beysens, Phys. Rev. A **41**, 2264 (1990).
[9] M.S. Giterman and V.A. Shteinberg, PMM **34**, 325 (1970).
[10] M. Assenheimer and V. Steinberg, Phys. Rev. Lett. **70**, 3888 (1993).
[11] A.B. Kogan, D. Murphy, and H. Meyer, Phys. Rev. Lett. **82**, 4635 (1999).
[12] P. Carlès and B. Ugurtas, Physica D **126**, 69 (1999).
[13] S. Chandrasekhar, *Hydrodynamic and Hydromagnetic Stability* (Clarendon Press, Oxford 1961).
[14] P. Carlès, Physica D **147**, 36 (2000).
[15] Y. Chiwata and A. Onuki, Phys. Rev. Lett. **87**, 144301 (2001).
[16] S. Amiroudine, P. Bontoux, P. Larroudé, B. Gilly, and B. Zappoli, J. Fluid Mech. **442**, 119 (2001).